

Received 6 July 2022, accepted 21 July 2022, date of publication 25 July 2022, date of current version 1 August 2022.

Digital Object Identifier 10.1109/ACCESS.2022.3193681

RESEARCH ARTICLE

5G Spatial Modeling of Personal RF-EMF Assessment Within Aircrafts Cabin Environments

MIKEL CELAYA-ECHARRI¹, (Graduate Student Member, IEEE),
 LEYRE AZPILICUETA¹, (Senior Member, IEEE),
 FIDEL ALEJANDRO RODRÍGUEZ-CORBO¹, (Student Member, IEEE),
 PEIO LOPEZ-ITURRI^{2,3}, RAED M. SHUBAIR⁴, (Senior Member, IEEE),
 VICTORIA RAMOS⁵, (Senior Member, IEEE),
 AND FRANCISCO FALCONE^{1,2,3}, (Senior Member, IEEE)

¹School of Engineering and Sciences, Tecnológico de Monterrey, Monterrey 64849, Mexico

²Electric, Electronic and Communication Engineering Department, Public University of Navarre, 31006 Pamplona, Spain

³Institute of Smart Cities, Public University of Navarre, 31006 Pamplona, Spain

⁴Department of Electrical and Computer Engineering, New York University (NYU) Abu Dhabi, Abu Dhabi, United Arab Emirates

⁵Telemedicine and eHealth Research Unit, Health Institute Carlos III, 28020 Madrid, Spain

Corresponding author: Leyre Azpilicueta (leyre.azpilicueta@tec.mx)

This work was supported by the Ministerio de Ciencia, Innovación y Universidades, Gobierno de España (MCIU/AEI/FEDER, UE) under Project RTI2018-095499-B-C31.

ABSTRACT Recently, new wireless communication systems within aircrafts cabins have drawn higher attention due to the growing demand of passenger services and applications and their corresponding requirements and constraints. In this regard, the fifth generation (5G) of wireless communication becomes an attractive and promising alternative to enable aircraft passengers' comfort and entertainment along the flight, considering its potential benefits in term of high data transfers and low latencies. Nevertheless, general population concern about radio frequency electromagnetic fields (RF-EMF) safety in general and, in particular to the environmental exposure at which we are all exposed in these flights, increases at the same time. Thus, in this work, we present an experimental campaign of measurements for current passengers' environmental exposure assessment, performed in different real generalizable type of flights and aircrafts' cabins, in order to provide current RF-EMF exposure insight within these complex heterogeneous environments. In addition, worst-case uplink 5G scenarios, where all 5G cellular handsets of the passengers operate at the same time, have been simulated by means of an in-house developed 3D Ray Launching (3D-RL) deterministic technique. Before takeoff and after landing, critical scenarios with the aircrafts' doors closed have been selected and assessed considering different types of modeled aircrafts full of passengers, considering 5G frequency range 2 (5G-FR2) operating links. The obtained results show that the operation frequency and the morphology and topology of the aircraft cabin have a great influence in the environmental RF-EMF passengers' spatial distribution and overall exposure, but not exceeding, even in worst case conditions, the international established regulatory limits.

INDEX TERMS Radiofrequency electromagnetic fields (RF-EMF), personal exposimeter (PEM), 3D ray launching (3D-RL), 5G, aircrafts.

NOMENCLATURE

LIST OF ACRONYMS

3D-RL Three-Dimensional Ray Launching.
 3GPP 3rd Generation Partnership Project.
 5G Fifth Generation.

5G-FR2 Fifth Generation Frequency Range 2.
 5G-NR Fifth Generation New Radio.
 BS Base Station.
 CDF Cumulative Distribution Function.
 CF Collaborative Filtering.
 DE Diffusion Equation.
 DL Downlink.
 EMC Electromagnetic Compatibility.

The associate editor coordinating the review of this manuscript and approving it for publication was Olutayo O. Oyerinde¹.

EMF	Electromagnetic Field.
EU	European Union.
FR1	Frequency Range 1.
FR2	Frequency Range 2.
GO	Geometrical Optics.
HD	High Density.
ICNIRP	International Commission on Non-Ionizing Radiation Protection.
KPI	Key Performance Indicator.
LD	Low Density.
LTE	Long Term Evolution.
MIMO	Multiple Input Multiple Output.
ML	Machine Learning.
MU	Multi-User.
NN	Neural Network.
PEM	Personal Exposimeter.
RF	Radio Frequency.
RF-EMF	Radio Frequency Electromagnetic Field.
RL	Ray Launching.
RX	Receiver.
SU	Single-User.
TDD	Time Division Duplex.
TX	Transmitter.
UE	User Equipment.
UL	Uplink.
USA	United States of America.
UTD	Uniform Theory of Diffraction.
UWB	Ultra-Wideband.

I. INTRODUCTION

With the growing demand of user service application requirements anywhere and anytime, wireless communications in aircraft cabins have widely attracted people attention. One of the reasons is that airplane passengers' desire to enjoy strong and secure in-flight personal wireless communication services with unlimited access to information data. In this sense, the fifth generation (5G) of wireless communication offers this unlimited access to information and sharing data [1]. Nowadays, many airline companies have offered wireless service access for aircraft cabins using terrestrial base station communication systems and satellite-based communication systems [2], [3]. However, with the incoming 5G technology, there is an increase population concern about radio frequency electromagnetic field (RF-EMF) exposure in general passengers as well as aircraft workers and staff. Electromagnetic fields (EMFs) can be roughly split into two important divisions, ionizing and non-ionizing electromagnetic radiation, depending on the system operating frequency [4]. The main important difference is that ionizing EMFs can break chemical bonds and thus cause radical changes in materials and biological tissues, while non-ionizing EMFs do not break chemical bonds, but they can cause heating owing to the contribution of the imaginary component of the electric permittivity. In the context of an aircraft cabin and flights, ionizing radiation is natural and comes from cosmic sources.

It can be referred as cosmic or galactic radiation, and the exposure intensity depends on the flight altitude, latitude, length of exposure, and time of the year [5]. On the one hand, over the years, several works have been assessed the ionizing radiation that passengers and staff can be exposed within aircraft cabins. In reference [6], an estimate of the total ionizing radiation dose received by the worldwide civilian flying population is presented. Other references [7], [8] present overviews of the different radiation exposure presented in the atmosphere and gives guidelines to aviation safety at large. On the other hand, the assessment of non-ionizing electromagnetic field radiation exposure within the aircraft cabins has had less attention in the literature over the years. In the context of aircraft cabins and flights, some sources of non-ionizing radiation exposure can be the interferences caused by the electronic devices/equipment within the aircraft or the passengers use of cellular handsets inside the cabin aircraft just before the takeoff or after landing (aircraft taxi mode). The work in [9] presents the assessment of the electromagnetic field produced by the equipment of three different training aircrafts and shows the comparison with the limits and the corresponding normative. The same aircrafts were used to analyze exposure in aircraft crew caused by radio navigation devices in [10]. The intensity of the electromagnetic field during one flight in high frequencies was also assessed in [11], showing results which did not reveal any exceedances of the permissible levels for these frequency ranges. Nevertheless, with the growing demand of wireless communication systems within these scenarios and the arrival of new technologies such as 5G, it becomes crucial to assess RF-EMF exposure in current flights as well as to estimate radiation exposure for next generation of wireless communication systems. 5G mobile communication systems provides data services at tens of Gbps, higher mobility range, lower latencies, and massive connectivity density devices when compared with previous generations. According to 3rd Generation Partnership Project (3GPP), the 5G New Radio (5G-NR) spectrum distinguishes between two ranges operating frequencies [12], which are:

- Frequency range 1 (FR1), which consists of the existing and new bands between 410 MHz to 7.125 GHz (including the frequency bands for Long Term Evolution (LTE)).
- Frequency range 2 (FR2), which consists of the new frequency bands (mmWave) range of 24.25 – 52.6 GHz.

The specific details of the operating bands and channel organization can be found in [13]. The mmWave spectrum (above 24 GHz) has been recently introduced for commercial use in mobile communications, with the main advantage of supporting high traffic demands with increased capacity in terms of data rates. However, mmWave spectrum suffers higher signal absorption and channel impairments, leading to an increase in the number of small cells in crowded scenarios. As a result of all these significant developments in technology, a considerable body of science is required, addressing

the relationship between radiofrequency EMFs and possible adverse health hazards. In this sense, short- and long-term, continuous, and discontinuous radiofrequency EMFs exposure scenarios must be rigorously analyzed, in order to provide high level protection for all users against substantiated adverse health effects [14].

Recently, several works in the literature have presented different models for the RF-EMF assessment of 5G communication systems. On the one hand, most of these works are focused on outdoor scenarios and present the EMF assessment focused on the downlink (DL) of a 5G system [15]–[18]. On the other hand, the works which present the EMF assessment of the uplink (UL) from the user equipment (UE) in a 5G system are usually focused on a unique user device and its interaction with the human body [19]–[22]. Nevertheless, less attention has been given in the literature to the assessment of human EMF exposure in complex heterogeneous crowded environments. In this regard, the passenger cabin of a commercial aircraft has distinctive characteristics in terms of radio wave propagation compared to typical indoor environments such as office environments, because of the special structure with relevant metallic clutter and high density of seating within it, which leads to have a high density of people in a confined volume. Although some research groups have characterized aircraft passenger cabins in terms of radio wave propagation for conventional wireless technologies [23] and ultra-wideband (UWB) [24]–[26], for the author's knowledge, nothing has been reported concerning RF-EMF personal exposure within commercial flights, and less considering 5G wireless communication systems.

The aim of this study is encouraged by the need to provide an accurate method to assess environmental occupational and general public RF-EMF exposure within complex generalizable aircrafts, including deterministic techniques to predict power density levels. Therefore, the main contributions are summarized as follows.

- 1) An in-house developed 3D-RL simulation tool for 5G EMF exposure assessment and dosimetric characterization within generalizable aircrafts is proposed.
- 2) From a complete analysis of different critical uplink 5G frequency range 2 (5G-FR2) case study scenarios within generalizable aircraft cabin models, it is demonstrated the unique and challenging spatial behavior regarding personal RF-EMF assessment and power density distribution levels within them.
- 3) In addition, to have clear insight into real onboard environmental RF-EMF personal exposure, a campaign of measurements is presented performed in different commercial flights of several durations, confirming current negligible values, when compared with the established regulatory limits.

The paper is organized as follows: Section II describes the system and simulation models, where the measurement setup is specified as well as the in-house developed enhanced RF-EMF exposure assessment simulation tool. Section III

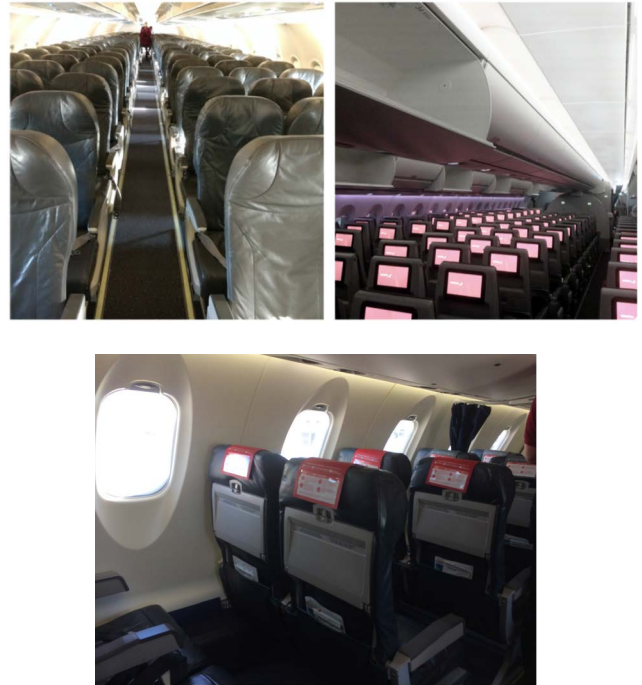


FIGURE 1. Real photos of the indoor area of the selected aircrafts.

TABLE 1. Main features of the selected aircrafts for the campaign of measurements.

Aircrafts	Indoor cabin dimensions	Indoor cabin distribution	Number of seats	Meas. seat
Intercontinental flight	(49.9, 6.5, 2.3) m	Rows of 10 seats with two aisles (3/4/3)	334	16C
Continental flight America	(32.5, 3.7, 2.3) m	Rows of 6 seats with an aisle (3/3)	168	14C
Continental flight EU	(27.6, 2.5, 1.8) m	Rows of 4 seats with an aisle (2/2)	50	12C

presents simulation and measurement results, as well as discussion. Finally, Section IV shows conclusions and future work.

II. SYSTEM AND SIMULATION MODELS

A. MEASUREMENT SETUP

An experimental campaign of measurements has been performed in order to provide clear insight of the real personal EMF exposure to which general flying public and occupational aircraft crew are exposed within commercial routine flights. For that purpose, an empirical environmental RF-EMF exposure assessment analysis is proposed considering worst case conditions in different types of challenging generalizable aircraft models with their corresponding specific cabins in terms of design, structure, morphology and



FIGURE 2. Real photo of the EME Spy evolution PEM within the measurement campaign in the aircraft.

topology. Specifically, measurements were continuously performed during all flights’ duration in full flights, with special emphasis in the considered worst-case conditions scenarios: before the takeoff and after landing, when RF electronic devices are allowed while the aircraft is closed. These are critical scenarios to evaluate EMF safety compliance with current international regulation limits.

The campaign of measurements was carried out in three different continental and inter-continental flights with their corresponding different aircrafts. Precisely, one flight was inter-continental flying from America to the European Union (EU), with a flight duration longer than eight hours, while the two others were continental flights (one of them in America and the other one in EU) with flight duration of approximately one hour. The inter-continental flight aircraft was an Airbus A380 model, while the American continental flight was an Airbus A320 model, and the EU continental flight was a Bombardier CRJ-1000 model. Real photos of the indoor cabin area of the selected aircrafts and their main features can be found in Fig. 1 and Table 1, respectively.

The characterization of environmental RF-EMF exposure within the aircrafts has been made by means of a frequency-selective exposure meter (known as exposimeter, or more precisely E-field exposimeter PEM). The main advantages of this measurement approach are its low cost, portability, and relatively easy use. Besides, PEMs are receiver/scanner devices that cannot transmit any signal, which was crucial to be used during flights, respecting the air regulations for the use of electronic devices on board and thus, ensuring safe operation mode, not interfering other communication systems or devices. The selected PEM device was an EME SPY Evolution frequency selective exposimeter (from Microwave Vision Group MVG, <https://www.mvg-world.com/es>), shown in Fig. 2 within the aircraft. The device is easily transported, pocket-size and battery powered. It measures environmental RF-EMF exposure levels over time, and it can be customizable in terms of predefined scenario region setups, sampling rate and frequency bands. The sensitivity of the EME SPY Evolution is 0.005 V/m in each individual frequency band and the E-field measurement range is 0.02-6 V/m. Moreover, the device is equipped with an

TABLE 2. Measurement settings.

Description	Value
Device	EME SPY Evolution
Device Sensitivity	0.005 V/m
Measurement Range	0.02-6 V/m
Scenario Region	USA / EU
Sampling Rate	5 seconds
Measured frequency bands	See Table 3
Device Location within the Aircraft	Aisle seat in the middle of the aircraft (See Table 1)
Intercontinental flight takeoff time recording	90 min
Intercontinental flight landing time recording	80 min
Continental flight America time recording	120 min
Continental flight EU time recording	70 min
Measurements dates	Dec. 2019–Jan. 2020

TABLE 3. USA and EU scenarios measured frequency bands of the EME Spy Evolution PEM device setup.

Scenario USA		Scenario EU	
Technology	Frequency (MHz)	Technology	Frequency (MHz)
FM US	88 - 108	FM	88 - 107
TV_VHF	174 - 223	TV_VHF	174 - 223
TV45	470 - 698	TETRA1	380 - 400
B12UL	699 - 716	TV45	470 - 698
B12DL	729 - 746	B28UL	703 - 748
B13DL	746 - 756	B28DL	758 - 803
B13UL	777 - 787	B20DL	791 - 821
B26UL	814 - 849	B20UL	832 - 862
B26DL	859 - 894	B8UL	880 - 915
ISM	902 - 928	B8DL	925 - 960
B4UL	1710 - 1755	B3UL	1710 - 1785
B25UL	1850 - 1915	B3DL	1805 - 1880
DECT6	1920 - 1930	DECT	1880 - 1900
B25DL	1930 - 1995	B1UL	1920 - 1980
B4DL	2110 - 2155	B1B10DL	2110 - 2170
B40TDD	2300 - 2400	B40 TDD	2300 - 2400
W2G	2400 - 2483	W2G	2400 - 2483
B7UL	2500 - 2570	B7UL	2500 - 2570
B7DL	2620 - 2690	B7DL	2620 - 2690
W5G	5150-5850	W5G	5150 - 5850

internal memory which allows more than 16K samples with the maximum recording sampling rate.

For this particular campaign of measurements, the specific region setups used correspond with the EU and United States of America (USA) predefined scenarios, based on the different measured flights: intercontinental from America to EU and continentals within America and EU. It must be remarked that the recording sampling rate is restricted according to the predefined region scenario setup. Specifically, measurements have been performed with the minimum measurement recording sampling rate allowed in both scenarios, which corresponds with a sampling rate of five seconds. Measurements were performed at frequencies below 6 GHz, due to the lack of current commercial PEM devices which

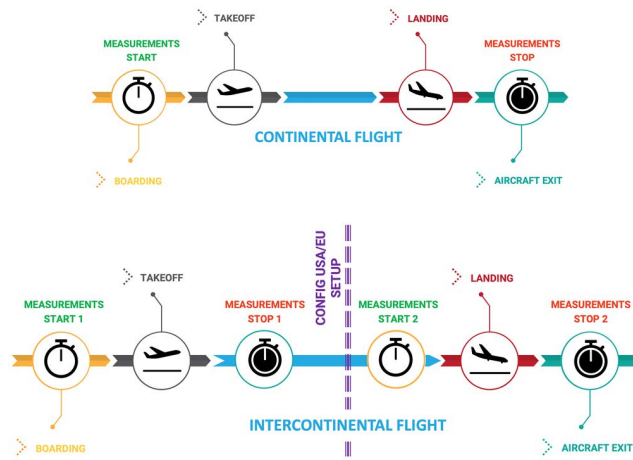


FIGURE 3. Timeline describing the measurement campaign procedure: continental flight (up) and intercontinental flight (down).

permit measurements at higher frequencies and the scarcity of mobile systems operating in these bands. The campaign of measurement settings in the different flights are presented in Table 2, and the measured frequency bands with the EME Spy Evolution PEM device for both scenarios are shown in Table 3.

The same measurement campaign procedure has been followed for all flights, regardless of the type of aircraft or the region. Fig. 3 presents the timeline description of the measurement campaign procedure. The main characteristics of the measurement campaign design were the following:

- For the continental flights, measurements have been performed continuously during the complete duration of all the flights, starting from the passenger boarding, the time of our entry to the plane, and finishing with the passenger departure, at the time of our exit from the plane.
- For the inter-continental flight (from America to EU), measurements have been performed continuously during the passenger boarding and takeoff with the USA predefined region scenario and landing and passenger departure with the EU predefined region setup.
- Measurements respected the normal routine of all the aircraft crew and passengers, with no interaction and without conditioning any passenger nor aircraft staff.
- Measurements' location during the flights was determined by the selected seat we had onboard, which was an aisle seat in the middle of the aircraft for all flights. It must be pointed out that all flights during the measurement campaign were full of passengers.
- The EME Spy Evolution PEM device was always located on the vicinity of the body, but not directly on the body, to avoid or at least decrease underestimation (only 1 V/m of body shielding effect when another user/scatterer is located between the radiating antenna and the receiver) [27].

B. SIMULATION MODEL

Different methodologies can be found in the literature that adequately characterize radio wave propagation channels, each of them with its advantages and disadvantages depending on the scenario and characteristics under consideration. These methodologies can be roughly divided into three categories. One category comprehends the empirical methods [28], [29], which are based on campaign of measurements in the considered scenario. They are characterized for its rapid computational time but cannot be generalized for other scenarios with different geometries and spatial characteristics. Another disadvantage of empirical approaches is that they can also be time and cost expensive.

A second category includes the stochastic methods [30], [31], which detail the statistical behavior of the channel characteristic parameters. From this category, two subcategories can be considered, the non-geometry based stochastic models and the geometry-based stochastic models, depending on the assumption or not of the underlying geometry of the environment. These methods are commonly used in non-stationary environments, such as the model presented in [32], which characterizes the time-changing statistics of high-speed vehicular environments.

However, when the surrounding environment of the considered scenario have a large impact on electromagnetic propagation, such as the case of the commercial aircraft cabin, because of the large number of scatterers within a confined small area and the material properties of the obstacles within it, a fourth category is considered, which comprehends the deterministic methods. Deterministic methods can be full wave approaches based on solving Maxwell's equations [33] or, approximations of them based on ray optics, such as ray tracing or ray launching techniques. Full wave deterministic methods are very accurate but also time-consuming for large environments, which can be unaffordable in realistic scenarios such as the commercial aircraft cabin. As a trade-off, ray tracing or ray launching techniques based on geometrical optics achieve a good accuracy with reasonable computational time for these complex scenarios [34], [35].

In this work, an enhanced in-house three-dimensional ray-launching (3D-RL) 5G-FR2 EMF simulation tool for different types of aircrafts is presented. The proposed methodology is based on reference [36], where the 3D-RL EMF exposure tool is presented for the radiation exposure analysis of different cellular technologies within public trams. A further step is proposed in this work, with the design, development, and implementation of a new module in the 3D-RL EMF simulation tool, which allows to recreate radio propagation channels considering multipath propagation within different generalizable full passengers' aircraft cabins for multiple 5G-FR2 communication links. In this sense, the enhanced EMF exposure tool enables the assessment of mmWave operating frequencies, with flexible beamforming and Single User/Multiple User (SU/MU) MIMO in both uplink (UL) and downlink (DL). The algorithm is based on geometrical optics (GO) and the Uniform Theory

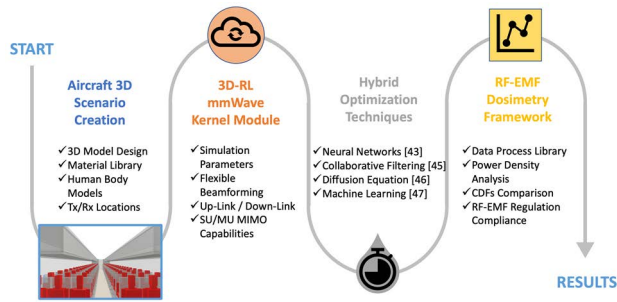


FIGURE 4. System model flowchart description.

of Diffraction (UTD) and comprises three stages. The first one is the creation of the scenario, where all the geometry and dimensions of the aircrafts are created in 3D considering the different material properties of all the obstacles within the environment. At this stage, parameters such as the transmitters and receivers' antenna locations and physical properties, operating frequency, number of rebounds, and rays angular and spatial resolution are defined. During the second stage, rays are launched from the transmitter antenna to the receiver. Electromagnetic phenomena, such as reflection, diffraction and refraction, are considered in this stage. During the last processing stage, the E-field is calculated for each spatial point of the scenario under consideration, following equation (1) [37].

$$P_R = \frac{E^2}{480\pi^2} \frac{c^2}{f^2} G_R, \quad (1)$$

where P_R is the received power in Watt, E is the E-field level in volts per m (V/m), $c = 3 \times 10^8$ m/s is the light speed, f is the frequency under analysis and G_R is the receiver antenna gain. From these results, the incident power density can be calculated as the modulus of the complex Poynting vector [38]:

$$S_{inc} = |\mathbf{E} \times \mathbf{H}^*|, \quad (2)$$

where \mathbf{E} is the E-field in V/m and \mathbf{H}^* is the complex conjugate of the magnetic field in amperes per m (A/m). In the case of the far field, the incident power density is derived as:

$$S_{inc} = \frac{|\mathbf{E}^2|}{Z_0} = Z_0 |\mathbf{H}^2|, \quad (3)$$

where Z_0 is the characteristic impedance of free space (i.e., $120\pi \Omega$).

The enhanced 3D-RL EMF tool permits the incorporation of human body models within the scenario under consideration. These models have been applied considering skin dielectric properties modularly [39]. The system model flowchart description is shown in Fig. 4 and the detailed information of the algorithm can be found in [40]. Following the same methodology as described in [41], [42], the proposed 3D-RL EMF algorithm provides an absolute mean error of 1-3 dB and a standard deviation of 1-6 dB, when compare with real measurements, as presented in [43], [44]. In addition, in order to decrease the computational time of the presented

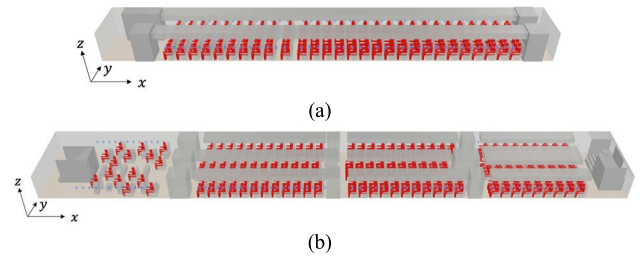


FIGURE 5. Rendered view of the two modeled aircrafts by means of the 3D-RL technique (a) Airbus A380, (b) Airbus A320.

algorithm, hybrid modeling approaches have been proposed combining the RL approach with different techniques, such as Neural Networks (NN) [43], Diffusion Equation (DE) [45], Collaborative Filtering (CF) [46] or Machine Learning (ML) techniques [47]. These hybrid methods achieve precise results whilst reducing the computational cost, leading to an Optimized 3D-RL approach, more efficient and robust for complex scenarios.

In addition, the potentiality to simulate UL and DL high-users density communication links within indoor complex environments can lead to the assessment of potential critical scenario situations, such as the landing of a commercial aircraft, where a large amount of people is confined in a small metallic area switching on the mobile phone at the same time. It must be pointed out that RL simulation results are uncertain in the near field region of the transmitter antenna. Thus, in order to avoid uncertain results in this area, an exclusion area of 5λ distance have been considered around the transmitter location based on the frequency under analysis [37].

In order to assess the potential critical scenario situations presented before, (i.e., the moment just after landing but before the opening airplane doors when passengers switch on their mobile phones at the same time), two different commercial aircraft cabins have been modeled in the 3D-RL EMF tool. These aircrafts correspond with an Airbus A380 and an Airbus A320, which are the same as the inter-continental aircraft and the America continental flight were the campaign of measurements has been performed, respectively. A realistic and detailed configuration, dimensions and aircraft's characteristics have been considered for both aircrafts, taking into account the positions of the seats depending on the class distribution within the aircraft, bathrooms, aisles, luggage compartments, and windows. Fig. 5 presents a detailed view of the two modeled cabin aircrafts. The A380 cabin aircraft has a $49.9 \text{ m} \times 6.58 \text{ m} \times 2.3 \text{ m}$ dimensions and a total of 334 seats for the first floor divided into four group of seats: first class, at the beginning of the plane with larger space between seats; second class in the following section, and finally two sections for tourist class in the last part of the cabin aircraft. The aircraft seats distribution consists of three seats on each side of the cabin and four seats in the middle, with two aisles between them. For the A320 aircraft, a total of 168 seats have been included with $32.5 \text{ m} \times 3.7 \text{ m} \times 2.3 \text{ m}$

TABLE 4. Different cases considered for simulation for the different aircrafts.

Scenario	System	5G-NR Band	Frequency	Active Users	
Airbus A320	5G-FR2	n257	28 GHz	LD _{A320}	84
				HD _{A320}	126
		n260	39 GHz	LD _{A320}	84
				HD _{A320}	126
Airbus A380	5G-FR2	n257	28 GHz	LD _{A380}	165
				HD _{A380}	248
		n260	39 GHz	LD _{A380}	165
				HD _{A380}	248

*LD/HD: Low Density (50% of users are active) / High Density (75% of users are active)

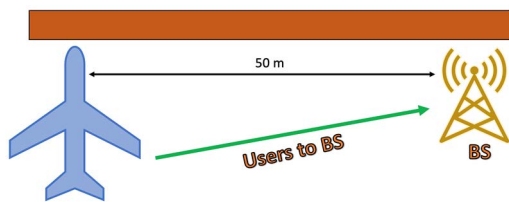


FIGURE 6. Schematic view of the considered simulation case study.

TABLE 5. Setting of main input parameters for 5G simulation setup in the considered scenario.

Description	Value	Ref
TX power per considered UE beam	15 dBm	[48]
Antenna type	Directional	
UE azimuth beam width	30°	[49]
UE elevation beam width	30°	[49]
UE antenna element gain	3 dBi	
F _{TDD}	0.75	[50, 51]
Carrier frequency	28/39 GHz	
3D-RL Angle Resolution	0.5°	
Number of reflections	4	
Scenarios	A320/A380	
Active users' densities	LD/HD	
Unitary volume analysis	0.2 m	

dimensions. The aircraft seats distribution is three seats on each side of the cabin with one aisle.

The objective of this work is to assess RF-EMF exposure within the cabin aircraft for 5G-FR2 technology at the specific moment just after landing but before the opening airplane doors, considering that the aircrafts are full of passengers, when different active users' densities are considered. Two different operating frequencies are considered for 5G-FR2 technology (28 and 39 GHz frequency bands) for both aircrafts. Besides, low, and high density (LD/HD) in terms of uplink active users have been considered to assess a realistic scenario where different number of passengers can be using their mobile phones. In LD, 50% of the total passengers of the aircraft are active, and in HD, 75% of the total passengers of the aircraft are active, for each aircraft

respectively. Table 4 presents the different cases considered for simulation, where two different aircrafts have been considered, with two different operating frequencies and two different active passengers within the aircrafts. Fig. 6 presents a schematic view of the considered uplink for simulation, where the base station (BS) is placed 50 meters at the right from the aircraft.

Each obstacle within the aircrafts has been modeled with its corresponding dimensions and electromagnetic material properties (considering the conductivity and relative permittivity) for the operating frequency under analysis. Table 5 shows the setting of the main input parameters used for each uplink active passenger within the aircrafts.

III. SIMULATION RESULTS

In most countries, EMF regulations and legislation and thus, RF-EMF radiation exposure limits, are based generally on the two most international adopted guidelines and standards [52], [53], the International Commission on Non-Ionizing Radiation Protection (ICNIRP) guidelines (ICNIRP 2020) [52], and the Institute of Electrical and Electronics Engineers (IEEE) standard C95.1-2019 by the IEEE International Committee on Electromagnetic Safety [53]. The new version of both guidelines was last updated in 2019 and 2020 respectively, accordingly with the health agencies and official entities. In both updated versions, the reference levels delimitation, or Key Performance Indicators (KPI) are defined in terms of power density for frequencies higher than 2 GHz and lower than 300 GHz for whole-body and far-field exposure conditions (which is the analyzed case presented in this work), with a maximum permitted of 50 W/m² and 10 W/m² for occupational and general public, respectively [52], [53].

A. AIRBUS A320

Firstly, the exposure assessment within the Airbus A320 aircraft model has been analyzed. In order to have insight into the power density levels within the aircraft, the cumulative distribution functions (CDF) have been depicted. Fig. 7 presents the power density CDF for the XYbi-dimensional plane of the passengers' head height when seated in the aircraft, considering both operating frequencies (28 and 39 GHz) and both user densities (HD and LD). Results show that for both operating frequencies, higher power density levels are obtained in the HD cases, yet lower than 0.3 W/m² for all spatial positions. Specifically, the difference between HD and LD is approximately of 0.05 W/m² higher for the HD case with a 90% probability at both operating frequencies. In addition, slightly higher power density levels for the higher frequency can also be observed, due to the smaller exclusion area of near field. Thus, spatial samples closer to the transmitter antenna are considered, leading to a CDF with slightly higher values at 39 GHz, yet for both frequency cases far below the current legislation limits.

In order to have clear insight of the power density levels spatial distribution within the aircraft when considering the HD case, in Fig. 8, the power density XY bi-dimensional

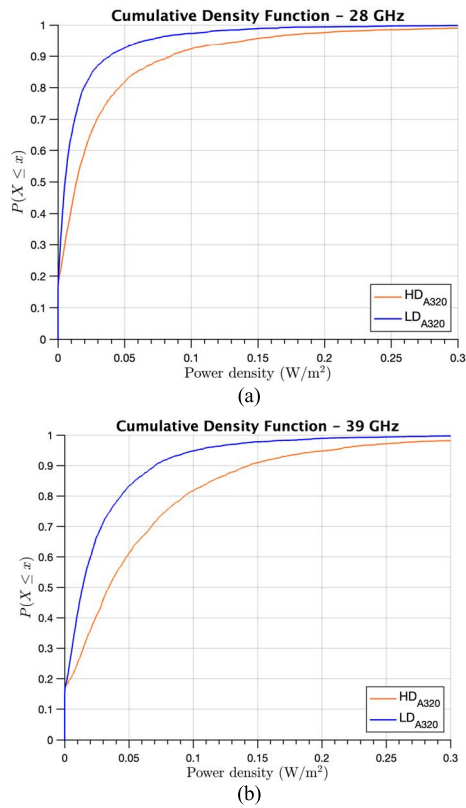


FIGURE 7. Power density CDFs for the XY bi-dimensional planes of the passengers' head height within the A320 aircraft for the HD and LD cases (a) 28 GHz frequency and (b) 39 GHz frequency.

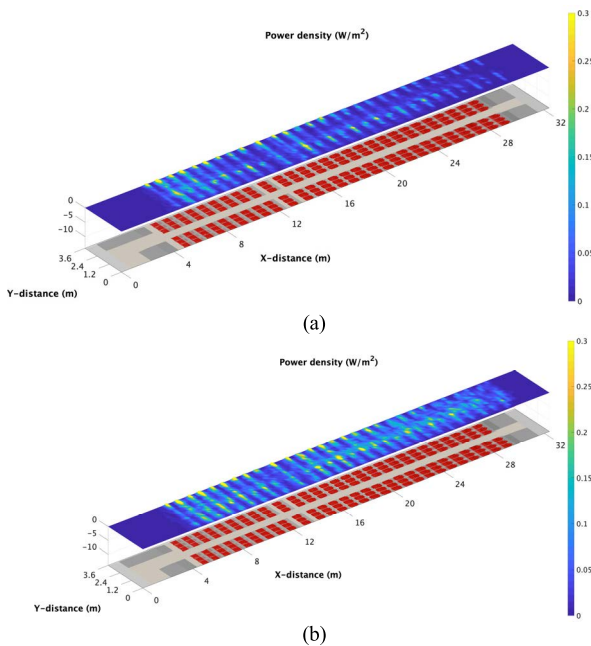


FIGURE 8. Power density XY bi-dimensional planes for the passengers' head height within the A320 aircraft for the HD case (a) 28 GHz frequency and (b) 39 GHz frequency.

planes at the same height (passengers' head height when seated in the aircraft) are presented. From the results

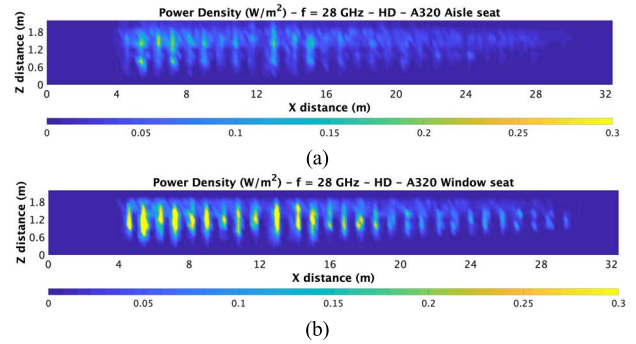


FIGURE 9. Power density XZ bi-dimensional planes for the A320 HD case at 28 GHz frequency (a) Right aisle seat row and (b) Right window seat row (see Figure 5 and 6 for reference).

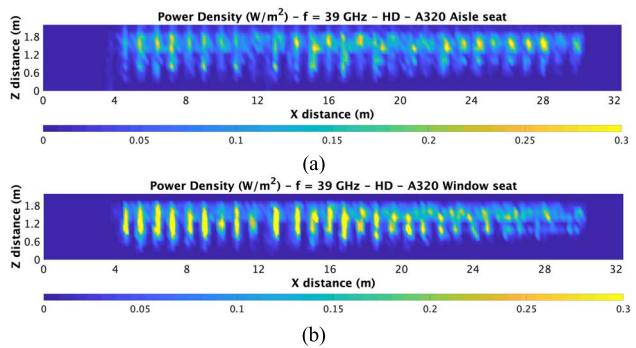


FIGURE 10. Power density XZ bi-dimensional planes for the A320 HD case at 39 GHz frequency (a) Right aisle seat row and (b) Right window seat row (see Figure 5 and 6 for reference).

obtained, it can be clearly observed that the highest power density levels are obtained in the window right seats locations. This is because all communication beams are focused on that direction, which is directly linked to the BS (placed at 50 m on the right side of the aircraft). Another spatial distribution pattern can be observed in the areas where the signal is confined between the rows of seats. These areas are more pronounced in the front right part of the aircraft due to the proximity to the BS (see Fig. 6 for reference). In both operating frequencies, the seats, and aircraft structure act as signal shielding, causing hot spots areas between seats, with highest values of 0.67 and 0.73 W/m² at 28 and 39 GHz respectively, both in the aircraft's front right area, closest to the BS, following the same distribution pattern trend. As in the CDF results, frequency impact is also observed, obtaining higher power density levels for the higher frequency, because the considered near field exclusion area is smaller in this case.

A further study is proposed, analyzing the vertical XZ bi-dimensional planes, to provide more information regarding the spatial distribution of the power density inside the aircraft. For that purpose, in Fig. 9 and Fig. 10, the vertical XZ planes on the right side of the aircraft, considering the window seat row and the aisle seat row at 28 GHz and 39 GHz respectively, are presented. For the first analyzed frequency, the difference of power density levels in the passenger head

for the aisle and window row seat can be clearly perceived. The exposure is concentrated in the window row seats, as this is the intersection area where all the direct connection links from all UEs to the BS. Therefore, confined exposure areas or hot spots could emerge due to the presence of obstacles, which behave as signal shielding in these challenging areas, instead of in the aisle seats, where the open space makes the signal tend to disperse. Besides, a remarkable signal concentration in the front area of the aircraft is presented as in previous results due to the proximity with the BS.

Analyzing the second frequency (39 GHz), the same exposure distribution trend is observed, showing a significant increase in terms of power density levels in the window seat rows. Comparing with the previous frequency case (28 GHz), slightly higher levels are captured, as the exclusion area is smaller due to the higher operating frequency. Besides, a more homogeneous distribution can be observed along the aircraft's body, with the highest power density levels at the passenger head height, much more concentrated in the window seat rows. At the same time, and given by the obstacles' presence, exposure concentrations or hot spots are presented in the confined row areas, as in the previous analysis. Nevertheless, the highest power density levels are well below the established regulation limits (10 W/m^2) [52], [53].

B. AIRBUS A380

Following, the exposure assessment analysis has been performed in a different aircraft's configuration. For this second study, an Airbus A380 has been selected, which is mainly characterized by being wider than the previous model and therefore, presenting a different seating arrangement. In this case, the aircraft has two aisles with a 3/4/3 passenger seating distribution for each row. It must be remarked that this new airplane scenario has been modeled in the simulation tool following the same structure, morphology, and dimensions as a real Airbus A380 aircraft (for instance, same distance between seats, toilets, compartments, different classes of passengers, spaces/areas in emergency exits, among others), following the same process as in the airbus A320 previous case.

To provide insight into radiation exposure levels within this aircraft, the power density levels within the complete volume of the scenario have been calculated. Fig. 11 presents the power density CDFs for the 28 and 39 GHz operating frequencies, as well as for HD and LD cases. Higher power density levels are obtained for both operating frequencies in the HD study case, as this case considers more active links within the aircraft. The larger dimensions in length and width of this second aircraft, cause wider opened areas, which in turn cause less signal confinement, showing lower power density levels when compared with the previous analyzed aircraft (A320). Thus, the obstacles density and distribution, as well as the aircraft morphology and topology have a great impact in RF-EMF exposure levels.

To have information about the spatial distribution of power density levels within the A380 aircraft, Fig. 12 presents the

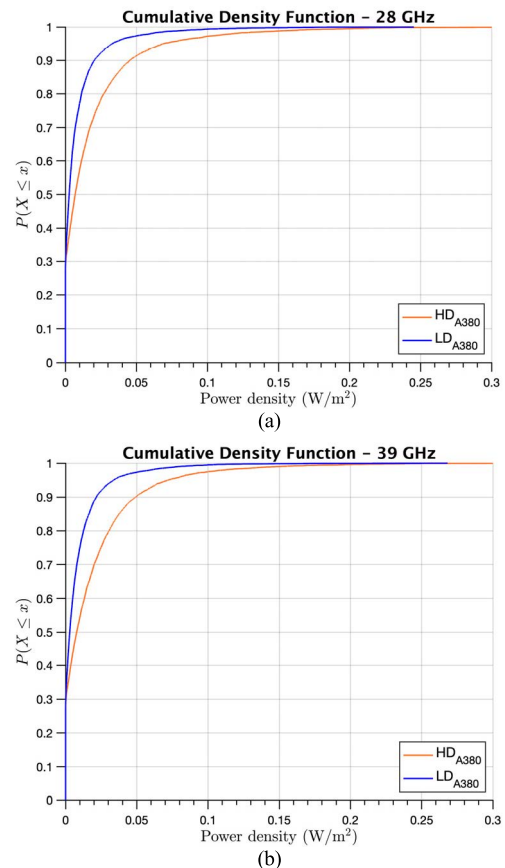


FIGURE 11. Power density CDFs for the XY bi-dimensional planes of the passengers' head height within the A380 aircraft for the HD and LD cases (a) 28 GHz frequency and (b) 39 GHz frequency.

XY bi-dimensional power density planes at the passengers' head height for 28 and 39 GHz frequencies. As in the previous case, a signal confinement is observed between the passengers' seats rows since the seats themselves with the passenger's act as a signal shielding. This can be clearly observed in the wider open areas, such as emergency exit zones, where power density levels drop considerably.

The highest power density levels in this case (A380) are 0.33 and 0.35 W/m^2 , for 28 and 39 GHz, respectively. These values are lower than the previous case (A320), showing the impact of the larger dimensions in width and length of this second aircraft, as well as the obstacles distribution within it.

As previously stated, the layout and obstacles distribution within the aircraft have a great influence in signal confinement. To further analyze this impact in the A380 aircraft, the vertical XZ bi-dimensional planes of the aisle and the window rows within the aircraft have been depicted in Fig. 13 and Fig. 14, for 28 and 39 GHz operating frequencies, respectively. From the results, slightly higher power density values are encountered in the window area, due to the closer proximity to the BS, rather than the aisle seats row. Nevertheless, the bigger dimensions and different seats distribution within the aircraft, cause a more evenly signal distribution,

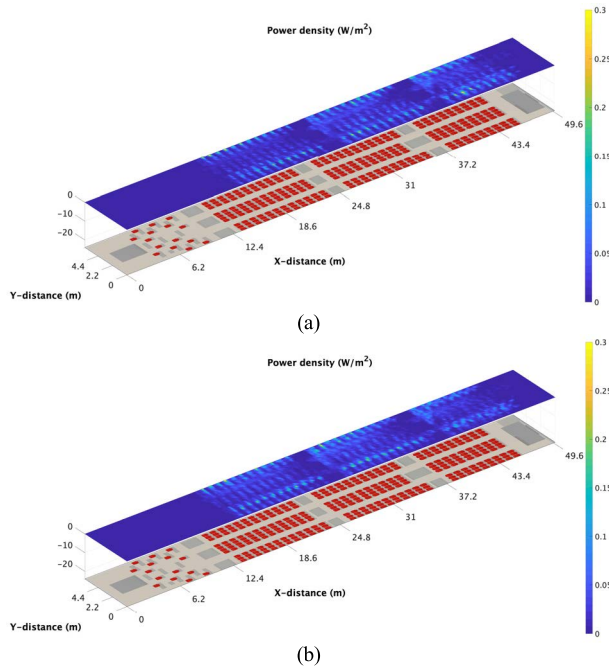


FIGURE 12. Power density XY bi-dimensional planes for the passengers' head height within the A380 aircraft for the HD case (a) 28 GHz frequency and (b) 39 GHz frequency.

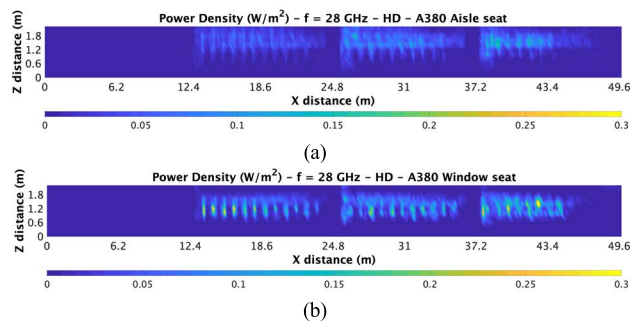


FIGURE 13. Power density XZ bi-dimensional planes for the A380 HD case at 28 GHz frequency (a) Right aisle seat row and (b) Right window seat row (see Figure 5 and 6 for reference).

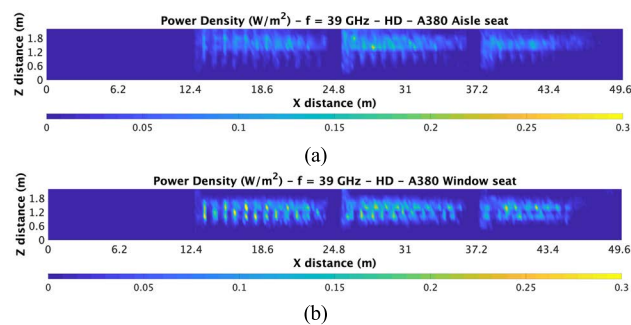


FIGURE 14. Power density XZ bi-dimensional planes for the A380 HD case at 39 GHz frequency (a) Right aisle seat row and (b) Right window seat row (see Figure 5 and 6 for reference).

resulting in lower power density levels than the previous analyzed case (A320). Nonetheless, in all cases, the values

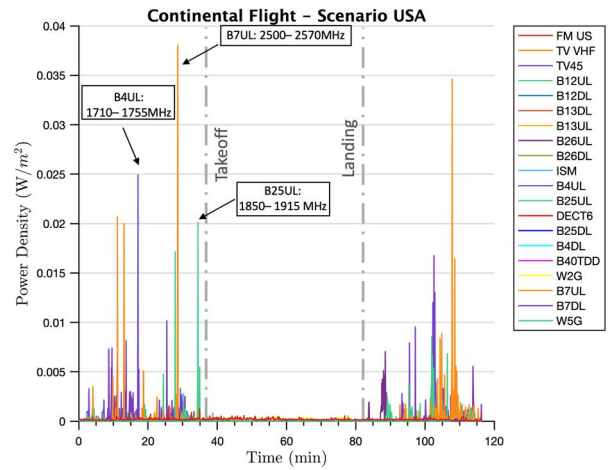


FIGURE 15. Power density results from the measurement campaign with the PEM during the continental flight in the American continent.

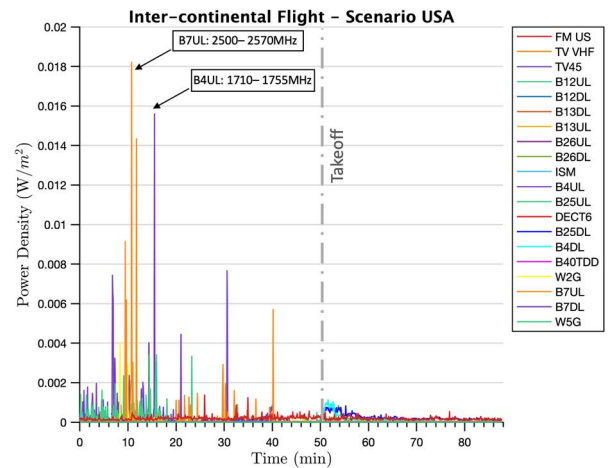


FIGURE 16. Power density results from the measurement campaign with the PEM during the takeoff of the inter-continental flight between the American continent and the European continent.

do not exceed the 7% of the maximum established limits [52], [53], even considering an indoor complex environment such as an aircraft, with unique and distinctive characteristics in terms of signal propagation.

IV. MEASUREMENT RESULTS

As it has been previously described in Section II.A, a campaign of measurements has been performed during three different continental/intercontinental flights as well as different types/models of aircrafts. The purpose of this empirical study is to provide clear insight of personal non-ionizing EMF exposure to which general public and aircraft crew are exposed during a flight, and specifically, considering worst-case conditions as the presented before the takeoff and after landing, when RF electronic devices are allowed while the aircraft is closed.

Firstly, Fig. 15 presents the measurement results for the continental flight within America. The main features of the aircrafts used for the measurement campaign can be seen in

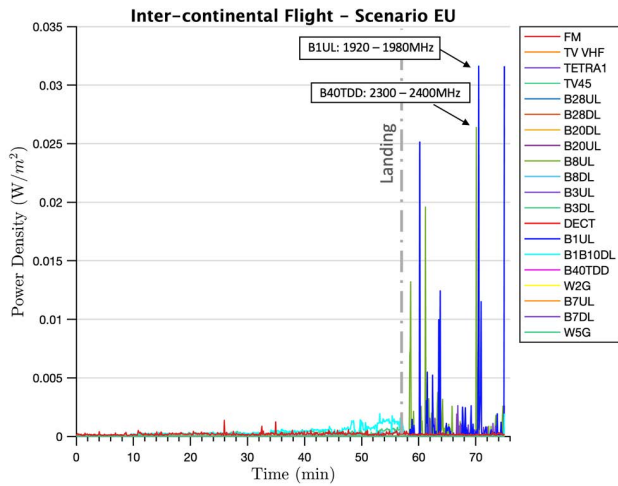


FIGURE 17. Power density results from the measurement campaign with the PEM during the landing of the inter-continental flight between the American continent and the European continent.

Table 1. The continental flight in America had a duration of 50 min approximately, while measurements were performed during 120 min, since the moment we were allowed to enter the aircraft to the moment we went out. Results clearly show that during the flight (i.e., after takeoff and before landing), power density levels are negligible. It is also noticeable that the higher measured power density levels before takeoff and after landing within the aircraft correspond with UL cellular frequency bands in all cases, with the highest measured power density level of 0.037 W/m^2 in the 2600 MHz frequency band.

Secondly, Fig. 16 and Fig. 17 present the measurement results for the inter-continental flight between America and Europe, where Fig. 16 shows measurements within the entrance to the aircraft and takeoff in America and Fig. 17 presents landing and aircraft departure measurements in Europe. As the continents are different, it can be noticed that the measured frequency bands were also different (see Table 3 for reference). From Fig. 16, it can be clearly observed that after takeoff, power density levels are negligible, and the main important measured levels before takeoff were UL cellular frequency bands, with a maximum of 0.018 W/m^2 in the 2600 MHz frequency band. Regarding the performed measurements in the same flight, in Fig. 17, the same flight trend with negligible power density levels before landing can be observed. Then, just after landing, it is noticeable the presence of higher power density levels, with a maximum of 0.031 W/m^2 which corresponds with an UL cellular frequency band at 1900 MHz.

Finally, Fig. 18 depicts the performed measurements within a continental flight of 40 min duration within Europe. It is noticeable that in this last case, the maximum peak of 0.037 W/m^2 was measured within the flight duration, at the 2300 – 2400 MHz frequency band, which is not an UL cellular frequency band, as in the previous cases.

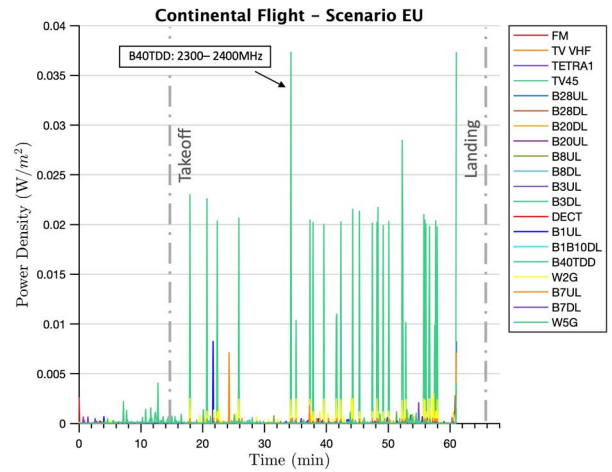


FIGURE 18. Power density results from the measurement campaign with the PEM during the continental flight in the European continent.

Nonetheless, all maximum measured peaks for all the different flights were below 0.037 W/m^2 , which is far below the established regulation limits (10 W/m^2) [52], [53].

V. CONCLUSION

In this work, the spatial modeling of the environmental general public and occupational RF-EMF exposure assessment in complex heterogeneous generalizable aircrafts environments has been presented considering 5G-FR2 worst case conditions in terms of passenger densities and simultaneous uplink operation. For that purpose, an in-house developed 3D-RL simulation tool for EMF exposure assessment and dosimetric characterization has been proposed, for the simulation of several critical 5G case study scenarios, considering different aircrafts cabin models as well as different high-node 5G uplink connection links operating at 28 and 39 GHz frequency bands.

Results show that confined complex heterogeneous environments such as aircrafts cabins, with a large content of metallic clutter within them, present a unique and challenging spatial behavior regarding the distribution of power density exposure levels. The narrow aircraft model (A320) presents slightly higher overall power density levels ($\sim 0.7 \text{ W/m}^2$) than the widest one (A380) ($\sim 0.3 \text{ W/m}^2$), due to the human body shielding effect and the high impact of the topology and obstacles density in a smaller area. While the morphology of both type of aircrafts' cabin design is relatively similar, the influence of the open space concept in the widest design (A380) versus a more limited/dedicated (A320) design has a great influence in the signal propagation behavior and the corresponding spatial exposure distribution. Nevertheless, power density exposure levels remain far below the international established regulatory limits (10 W/m^2) [52],[53], even considering critical scenarios with the aircrafts full of passengers in worst-case operation conditions.

Finally, an experimental campaign of measurements performed in three different commercial flights (continental in

USA, inter-continental between USA and EU, and continental in EU) have been included in order to provide clear and real onboard environmental RF-EMF exposure insight. Measured results confirm critical scenarios: just before the takeoff and after landing; with negligible highest EMF power density exposure levels rounding 0.037 W/m^2 .

It must be remarked that RF-EMFs may also interfere with electrical components or equipment, referred as electromagnetic compatibility (EMC), which can potentially affect human health indirectly due to possible malfunctions (on body e-health wireless solutions or active implantable medical devices, among others). Such effects depend on numerous EMF factors and conditions, including frequency, signal level, polarization or distribution in space and time. In this regard, stringent and strict international legislation and regulations, standards, and guidelines, in terms of EMC interference management, manufacturing and exposure conditions [54]–[57] were issued to set out the minimum requirements for the protection of occupational and general public health and safety, regarding a defined set of direct and indirect biophysical effects of EMF exposure at frequencies ranging from 0–300 GHz. Emissions, exposure, or interferences from 5G-FR2 wireless communication solutions, as the presented in this work, are far below the aforementioned limits even in worst-case conditions. Affection or possible effects on aircraft navigation (instrumentation of avionics) is negligible as well, due to their inherent use characteristics in term of frequency and power.

In general, the proposed 3D-RL simulation tool for RF-EMF exposure assessment can potentially assess critical complex heterogeneous environments and predict in advance exposure distributions and levels considering different scenario morphologies and topologies as well as different passenger densities and operation conditions. Consequently, the presented in-depth results can aid to calm down the general flight population and occupational crew concern regarding the non-ionizing radiation exposure within flights and specifically, to settle down the basis about 5G in-flight personal wireless communication services and applications as well as radiation exposure distributions and levels within different generalizable aircrafts' cabin models.

REFERENCES

- [1] C.-X. Wang, F. Haider, X. Gao, X.-H. You, Y. Yang, D. Yuan, H. Aggoune, H. Haas, S. Fletcher, and E. Hepsaydir, "Cellular architecture and key technologies for 5G wireless communication networks," *IEEE Commun. Mag.*, vol. 52, no. 2, pp. 122–130, Feb. 2014.
- [2] T. Cogalan, S. Videv, and H. Haas, "Operating an in-cabin femto-cellular system within a given LTE cellular network," *IEEE Trans. Veh. Technol.*, vol. 67, no. 8, pp. 7677–7689, Aug. 2018.
- [3] T. Cogalan, S. Videv, and H. Haas, "Inflight connectivity: Deploying different communication networks inside an aircraft," in *Proc. IEEE 87th Veh. Technol. Conf. (VTC Spring)*, Jun. 2018, pp. 1–6.
- [4] (Accessed: Nov. 11, 2021). *EU-Funded Research Into the Impact of Electromagnetic Fields and Mobile Telephones on Health. European Commission Community Research*. [Online]. Available: https://ec.europa.eu/health/archive/ph_determinants/environment/emf/brochure_en.pdf
- [5] J. J. Aw, "Cosmic radiation and commercial air travel," *J. Travel Med.*, vol. 10, no. 1, pp. 19–28, Mar. 2006.
- [6] L. E. Alvarez, S. D. Eastham, and S. R. H. Barrett, "Radiation dose to the global flying population," *J. Radiol. Protection*, vol. 36, p. 93, Jan. 2016.
- [7] C. A. Federico, O. L. González, G. M. A. A. Sordi, and L. V. E. Caldas, "Effects of cosmic radiation in aircrafts: A discussion about aircrew over South America," *J. Aerosp. Technol. Manag.*, vol. 4, no. 2, pp. 219–225, Apr.–Jun., 2012.
- [8] M. M. Meier, K. Copeland, K. E. J. Klöble, D. Matthäi, M. C. Plettenberg, K. Schennetten, M. Wirtz, and C. E. Hellweg, "Radiation in the atmosphere—A hazard to aviation safety?" *Atmosphere*, vol. 11, no. 12, p. 1358, Dec. 2020.
- [9] J. Michalowska, J. Pytka, A. Tofil, J. Jozwik, L. Puzio, and P. Krupski, "The assessment of electromagnetic field in commonly used training aircrafts," in *Proc. IEEE 7th Int. Workshop Metrol. Aerosp. (MetroAeroSpace)*, Jun. 2020, pp. 249–254, doi: [10.1109/MetroAeroSpace48742.2020.9160098](https://doi.org/10.1109/MetroAeroSpace48742.2020.9160098).
- [10] J. Michalowska, J. Pytka, A. Tofil, P. Krupski, and L. Puzio, "Assessment of training aircraft crew exposure to electromagnetic fields caused by radio navigation devices," *Energies*, vol. 14, no. 1, p. 254, Jan. 2021, doi: [10.3390/en14010254](https://doi.org/10.3390/en14010254).
- [11] J. Michalowska, J. Jozwik, and A. Tofil, "Monitoring of the intensity of the electromagnetic field during the aircraft operation in the field of high frequencies," in *Proc. IEEE 5th Int. Workshop Metrol. Aerosp. (MetroAeroSpace)*, Jun. 2019, pp. 366–370, doi: [10.1109/MetroAeroSpace.2019.8869638](https://doi.org/10.1109/MetroAeroSpace.2019.8869638).
- [12] *5G; NR; Base Station (BS) Radio Transmission and Reception (Release 15)*, document 3GPP, TS 138 104 V15.5, 2019, pp. 1–219.
- [13] *NR; User Equipment (UE) Radio Transmission and Reception; Part 1: Range 1 Standalone (Release 16)*, document 3GPP, Tech. Spec. V16.0.0, 2019, pp. 1–268.
- [14] World Health Organization (WHO). Fact Sheet. (Oct. 2013). *Electromagnetic Fields and Public Health: Mobile Phones*. [Online]. Available: <http://www.who.int/>
- [15] L. Chiaraviglio, S. Rossetti, S. Saida, S. Bartoletti, and N. Blefari-Melazzi, "Pencil beamforming increases human exposure to ElectroMagnetic fields': True or false?" *IEEE Access*, vol. 9, pp. 25158–25171, 2021, doi: [10.1109/ACCESS.2021.3057237](https://doi.org/10.1109/ACCESS.2021.3057237).
- [16] S. Shikhantsov, A. Thielens, S. Aerts, L. Verloock, G. Torfs, L. Martens, P. Demeester, and W. Joseph, "Ray-tracing-based numerical assessment of the spatiotemporal duty cycle of 5G massive MIMO in an outdoor urban environment," *Appl. Sci.*, vol. 10, no. 21, p. 7631, Oct. 2020, doi: [10.3390/app10217631](https://doi.org/10.3390/app10217631).
- [17] S. Shikhantsov, A. Thielens, G. Vermeeren, E. Tanghe, P. Demeester, L. Martens, G. Torfs, and W. Joseph, "Hybrid ray-tracing/FDTD method for human exposure evaluation of a massive MIMO technology in an industrial indoor environment," *IEEE Access*, vol. 7, pp. 21020–21031, 2019, doi: [10.1109/ACCESS.2019.2897921](https://doi.org/10.1109/ACCESS.2019.2897921).
- [18] M. Matalatala Tamasala, S. Shikhantsov, M. Deruyck, E. Tanghe, D. Plets, S. K. Goudos, L. Martens, and W. Joseph, "Combined ray-tracing/FDTD and network planner methods for the design of massive MIMO networks," *IEEE Access*, vol. 8, pp. 206371–206387, 2020, doi: [10.1109/ACCESS.2020.3035317](https://doi.org/10.1109/ACCESS.2020.3035317).
- [19] W. He, B. Xu, L. Scialacqua, Z. Ying, A. Scannavini, L. J. Foged, K. Zhao, C. Di Paola, S. Zhang, and S. He, "Fast power density assessment of 5G mobile handset using equivalent currents method," *IEEE Trans. Antennas Propag.*, vol. 69, no. 10, pp. 6857–6869, Oct. 2021, doi: [10.1109/TAP.2021.3070725](https://doi.org/10.1109/TAP.2021.3070725).
- [20] S. S. Zhekov, K. Zhao, O. Franek, and S. Zhang, "Test reduction for power density emitted by handset mmWave antenna arrays," *IEEE Access*, vol. 9, pp. 23127–23138, 2021, doi: [10.1109/ACCESS.2021.3055420](https://doi.org/10.1109/ACCESS.2021.3055420).
- [21] B. Xu, K. Zhao, Z. Ying, D. Sjöberg, W. He, and S. He, "Analysis of impacts of expected RF EMF exposure restrictions on peak EIRP of 5G user equipment at 28 GHz and 39 GHz bands," *IEEE Access*, vol. 7, pp. 20996–21005, 2019, doi: [10.1109/ACCESS.2019.2897271](https://doi.org/10.1109/ACCESS.2019.2897271).
- [22] N. Chahat, M. Zhadobov, L. Le Coq, S. I. Alekseev, and R. Sauleau, "Characterization of the interactions between a 60-GHz antenna and the human body in an off-body scenario," *IEEE Trans. Antennas Propag.*, vol. 60, no. 12, pp. 5958–5965, Dec. 2012, doi: [10.1109/TAP.2012.2211326](https://doi.org/10.1109/TAP.2012.2211326).
- [23] J. Wen, Y. Zhang, G. Yang, Z. He, and W. Zhang, "Path loss prediction based on machine learning methods for aircraft cabin environments," *IEEE Access*, vol. 7, pp. 159251–159261, 2019, doi: [10.1109/ACCESS.2019.2950634](https://doi.org/10.1109/ACCESS.2019.2950634).
- [24] S. Chiu, J. Chuang, and D. G. Michelson, "Characterization of UWB channel impulse responses within the passenger cabin of a Boeing 737–200 aircraft," *IEEE Trans. Antennas Propag.*, vol. 58, no. 3, pp. 935–945, Mar. 2010, doi: [10.1109/TAP.2009.2037707](https://doi.org/10.1109/TAP.2009.2037707).

- [25] S. Chiu and D. G. Michelson, "Effect of human presence on UWB radiowave propagation within the passenger cabin of a midsize airliner," *IEEE Trans. Antennas Propag.*, vol. 58, no. 3, pp. 917–926, Mar. 2010, doi: 10.1109/TAP.2009.2039326.
- [26] J. Chuang, N. Xin, H. Huang, S. Chiu, and D. G. Michelson, "UWB radiowave propagation within the passenger cabin of a Boeing 737–200 aircraft," in *Proc. IEEE 65th Veh. Technol. Conf.*, Apr. 2007, pp. 496–500, doi: 10.1109/VETECS.2007.113.
- [27] M. Celaya-Echarri, L. Azpilicueta, P. Lopez-Iturri, E. Aguirre, S. De Miguel-Bilbao, V. Ramos, and F. Falcone, "Spatial characterization of personal RF-EMF exposure in public transportation buses," *IEEE Access*, vol. 7, pp. 33038–33054, 2019.
- [28] Z. E. Khaled, W. Ajib, and H. Mcheick, "An accurate empirical path loss model for heterogeneous fixed wireless networks below 5.8 GHz frequencies," *IEEE Access*, vol. 8, pp. 182755–182775, 2020.
- [29] N. Faruk, S. I. Popoola, N. T. Surajudeen-Bakinde, A. A. Oloyede, A. Abdulkarim, M. Ali, C. T. Calafate, A. A. Atayero, and L. A. Olawoyin, "Path loss predictions in the VHF and UHF bands within urban environments: Experimental investigation of empirical, heuristics and geospatial models," *IEEE Access*, vol. 7, pp. 77293–77307, 2019.
- [30] A. F. Molisch, F. Tufvesson, J. Karedal, and C. F. Mecklenbrauker, "A survey on vehicle-to-vehicle propagation channels," *IEEE Wireless Commun.*, vol. 16, no. 6, pp. 12–21, Dec. 2009.
- [31] L. Cheng, D. D. Stancil, and F. Bai, "A roadside scattering model for the vehicle-to-vehicle communication channel," *IEEE J. Sel. Areas Commun.*, vol. 31, no. 9, pp. 449–459, Sep. 2013.
- [32] A. Ghazal, C.-X. Wang, B. Ai, D. Yuan, and H. Haas, "A nonstationary wideband MIMO channel model for high-mobility intelligent transportation systems," *IEEE Trans. Intell. Transp. Syst.*, vol. 16, no. 2, pp. 885–897, Apr. 2015.
- [33] Z. El Ahdab and F. Akleman, "An efficient 3-D FDTD-PE hybrid model for radio wave propagation with near-source obstacles," *IEEE Trans. Antennas Propag.*, vol. 67, no. 1, pp. 346–355, Jan. 2019.
- [34] M. M. Taygur and T. F. Eibert, "A ray-tracing algorithm based on the computation of (Exact) ray paths with bidirectional ray-tracing," *IEEE Trans. Antennas Propag.*, vol. 68, no. 8, pp. 6277–6286, Aug. 2020.
- [35] S. Hussain and C. Brennan, "Efficient preprocessed ray tracing for 5G mobile transmitter scenarios in urban microcellular environments," *IEEE Trans. Antennas Propag.*, vol. 67, no. 5, pp. 3323–3333, May 2019.
- [36] M. Celaya-Echarri, L. Azpilicueta, J. Karpowicz, V. Ramos, P. Lopez-Iturri, and F. Falcone, "From 2G to 5G spatial modeling of personal RF-EMF exposure within urban public trams," *IEEE Access*, vol. 8, pp. 100930–100947, 2020.
- [37] S. Salous, *Radio Propagation Measurement and Channel Modelling*. Hoboken, NJ, USA: Wiley, 2013.
- [38] M. Born and E. Wolf, *Principles of Optics: Electromagnetic Theory of Propagation, Interference and Diffraction of Light*. Amsterdam, The Netherlands: Elsevier, 2013.
- [39] E. Aguirre, J. Arpon, L. Azpilicueta, S. De Miguel Bilbao, V. Ramos, and F. Falcone, "Evaluation of electromagnetic dosimetry of wireless systems in complex indoor scenarios with human body interaction," *Prog. Electromagn. Res. B*, vol. 43, pp. 189–209, 2012.
- [40] L. Azpilicueta, M. Rawat, K. Rawat, F. Ghannouchi, and F. Falcone, "Convergence analysis in deterministic 3D ray launching radio channel estimation in complex environments," *ACES J.*, vol. 29, no. 4, pp. 256–271, Apr. 2014.
- [41] L. Azpilicueta, P. López-Iturri, E. Aguirre, C. Vargas-Rosales, A. León, and F. Falcone, "Influence of meshing adaption in convergence performance of deterministic ray launching estimation in indoor scenarios," *J. Electromagn. Waves Appl.*, vol. 31, no. 5, pp. 544–559, Mar. 2017.
- [42] L. Azpilicueta, E. Aguirre, P. López-Iturri, and F. Falcone, "An accurate UTD extension to a ray-launching algorithm for the analysis of complex indoor radio environments," *J. Electromagn. Waves Appl.*, vol. 30, no. 1, pp. 43–60, Jan. 2016.
- [43] L. Azpilicueta, M. Rawat, K. Rawat, F. Ghannouchi, and F. Falcone, "A ray launching-neural network approach for radio wave propagation analysis in complex indoor environments," *IEEE Trans. Antennas Propag.*, vol. 62, no. 5, pp. 2777–2786, May 2014.
- [44] L. Azpilicueta, F. Falcone, and R. Janaswamy, "Hybrid computational techniques: Electromagnetic propagation analysis in complex indoor environments," *IEEE Antennas Propag. Mag.*, vol. 61, no. 6, pp. 20–30, Dec. 2019.
- [45] L. Azpilicueta, F. Falcone, and R. Janaswamy, "A hybrid ray launching-diffusion equation approach for propagation prediction in complex indoor environments," *IEEE Antennas Wireless Propag. Lett.*, vol. 16, pp. 214–217, 2016.
- [46] F. Casino, P. Lopez-Iturri, E. Aguirre, L. Azpilicueta, F. Falcone, and A. Solanas, "Enhanced wireless channel estimation through parametric optimization of hybrid ray launching-collaborative filtering technique," *IEEE Access*, vol. 8, pp. 83070–83080, 2020.
- [47] M. Diago-Mosquera, A. Aragon-Zavala, L. Azpilicueta, R. Shubair, and F. Falcone, "A 3-D indoor analysis of path loss modeling using Kriging techniques," *IEEE Antennas Wireless Propag. Lett.*, vol. 21, no. 6, pp. 1218–1222, Jun. 2022.
- [48] B. Thors, D. Colombi, Z. Ying, T. Bolin, and C. Törnevik, "Exposure to RF EMF from array antennas in 5G mobile communication equipment," *IEEE Access*, vol. 4, pp. 7469–7478, 2016.
- [49] A. T. Nassar, A. I. Sulymán, and A. Alsaní, "Radio capacity estimation for millimeter wave 5G cellular networks using narrow beamwidth antennas at the base stations," *Int. J. Antennas Propag.*, vol. 2015, pp. 1–6, 2015, doi: 10.1155/2015/878614.
- [50] B. Thors, A. Furuskär, D. Colombi, and C. Törnevik, "Time-averaged realistic maximum power levels for the assessment of radio frequency exposure for 5G radio base stations using massive MIMO," *IEEE Access*, vol. 5, pp. 19711–19719, 2017, doi: 10.1109/ACCESS.2017.2753459.
- [51] S. Adda, T. Aureli, S. D'Elia, D. Franci, E. Grillo, M. D. Migliore, S. Pavoncello, F. Schettino, and R. Suman, "A theoretical and experimental investigation on the measurement of the electromagnetic field level radiated by 5G base stations," *IEEE Access*, vol. 8, pp. 101448–101463, 2020, doi: 10.1109/ACCESS.2020.2998448.
- [52] ICNIRP, "Guidelines for limiting exposure to electromagnetic fields (100 kHz to 300 GHz)," *Health Phys.*, vol. 118, no. 5, pp. 483–524, May 2020.
- [53] *IEEE Approved Draft Standard for Safety Levels With Respect to Human Exposure to Electric, Magnetic and Electromagnetic Fields, 0Hz to 300 GHz*, Standard IEEE C95.1, no. 2, 2019.
- [54] *Directive of the European Parliament and of the Council of 26, June 2013 on the Minimum Health and Safety Requirements Regarding the Exposure of Workers to the Risks Arising From Physical Agents (Electromagnetic Fields) (20th Individual Directive Within the Meaning of Article 16(1) of Directive 89/391/EEC)*, O.J. No. L-179 of 29, document Directive 2013/35/EU, Brussels, Belgium, Jun. 2013.
- [55] *Medical Electrical Equipment—Part 1-2: General Requirements for Basic Safety and Essential Performance—Collateral Standard: Electromagnetic Disturbances—Requirements and Tests*. Brussels: CENELEC [European Committee for Electrotechnical Standardization], Standard EN 60601-1-2:2015/A1:2021, 2021.
- [56] *Procedure for the Assessment of the Exposure to Electromagnetic Fields of Workers Bearing Active Implantable Medical Devices—Part 1: General*. Brussels: CENELEC [European Committee for Electrotechnical Standardization], Standard EN 50527-1:2016, 2016.
- [57] (Jul. 30, 1999). *European Council. Council Recommendation of 12 Jul. 1999 on the Limitation of Exposure of the General Public to Electromagnetic Fields (0 Hz to 300 GHz)—(1999/519/EC)*. *Official Journal of the European Communities L 199/59*. Accessed: Jul. 6, 2022. [Online]. Available: <https://eur-lex.europa.eu/LexUriServ/LexUriServ.do?uri=OJ:L:1999:199:0059:0070:EN:PDF>



MIKEL CELAYA-ECHARRI (Graduate Student Member, IEEE) received the Computer Science Engineering and M.Sc. degrees in project management from the Public University of Navarre (UPNA), in 2011 and 2015, respectively, and the Ph.D. degree in engineering and sciences from Tecnológico de Monterrey, Mexico, in 2022. From 2011 to 2014, he worked as a Research and Development Engineer at Tafco Metawireless, Spain. From 2015 to 2017, he was a Visiting Research Assistant with the Networks and Telecommunications Research Group, Tecnológico de Monterrey, where he is currently working as a Postdoctoral Researcher. His research interests include radio frequency electromagnetic dosimetry, radio propagation, wireless sensor networks, project management, and computer science.



LEYRE AZPILICUETA (Senior Member, IEEE) received the degree in telecommunications engineering, the master's degree in communications, and the Ph.D. degree in telecommunication technologies from the Public University of Navarre (UPNA), Spain, in 2009, 2011, and 2015, respectively. In 2010, she worked as a Radio Engineer with the Research and Development Department, RFID Osés. She is currently working as an Associate Professor and a Researcher at Tecnológico de Monterrey, Campus Monterrey, Mexico. She has over 250 contributions in relevant journals and conference publications. She has coauthored the textbook *Radio Wave propagation in Vehicular Environments* (2020), from The Institution of Engineering and Technology. Her research interests include radio propagation, mobile radio systems, wireless sensor networks, ray tracing, and channel modeling. She has received numerous awards and recognitions over the past few years, including the IEEE Antennas and Propagation Society Doctoral Research Award 2014, the Young Professors and Researchers Santander Universities 2014 Mobility Award, the ECSA 2014 Best Paper Award, the IISA 2015 Best Paper Award, the Best Ph.D. in 2016 awarded by the Colegio Oficial de Ingenieros de Telecomunicación, the IEEE N2Women: Rising Stars in Computer Networking and Communications 2018 Award, ISSI 2019 Best Paper Award, EAI IndustrialIoT 2020 Best Paper Award, IEEE Junior Research Raj Mittra Travel Grant 2020, Distinguished Professor Award 2020 and 2021, and IEEE Mojgan Daneshmand Grant 2021. She is the IEEE Communications Society Monterrey Chapter Chair and a Faculty Advisor of the IEEE-HKN Lambda-Rho Chapter. She has been on the Editorial Board of the IEEE SENSORS LETTERS, since 2020, and *International Journal of Electronics and Communications*, since 2018.



FIDEL ALEJANDRO RODRÍGUEZ-CORBO (Student Member, IEEE) received the degree in telecommunications and electronics engineering from the University of Pinar del Río (UPR), Cuba, in 2012, and the master's degree in electronic systems design from the Technological University of Havana, in 2018. He is currently pursuing the Ph.D. degree in engineering science with the Networks and Telecommunications Research Group, Tecnológico de Monterrey, Mexico. From 2015 to 2018, he worked as an Associate Professor with the Department of Telecommunications, Technological University of Havana. His research interests include radio propagation, wireless sensor networks, embedded systems, and digital signal processing.



PEIO LOPEZ-ITURRI received the degree in telecommunications engineering, the master's degree in communications, and the Ph.D. degree in communication engineering from the Public University of Navarre (UPNA), Pamplona, Navarre, in 2011, 2012, and 2017, respectively. Since 2019, he has been partly working as a Researcher with Tafco Metawireless. He is currently affiliated with the Institute for Smart Cities (ISC), UPNA. He worked in ten different public and privately funded research projects. He has more than 120 contributions in indexed international journals, book chapters, and conference contributions. His research interests include radio propagation, wireless sensor networks,

electromagnetic dosimetry, modeling of radio interference sources, mobile radio systems, wireless power transfer, the IoT networks and devices, 5G communication systems, and EMI/EMC. He received the 2018 Best Spanish Ph.D. Thesis in Smart Cities in CAEPIA 2018 (3rd prize), sponsored by the Spanish network on research for Smart Cities CI-RTI and Sensors (ISSN 1424-8220). He was a recipient the ECSA 2014 Best Paper Award, the IISA 2015 Best Paper Award, and the ISSI 2019 Best Paper Award.



RAED M. SHUBAIR (Senior Member, IEEE) received the B.Sc. degree (Hons.) in electrical engineering from Kuwait University, Kuwait, in June 1989, and the Ph.D. degree (Hons.) in electrical engineering from the University of Waterloo, Canada, in February 1993. He is currently a Full Professor of electrical engineering affiliated with New York University (NYU) Abu Dhabi. His current and past academic and research appointments also include the Massachusetts Institute of Technology (MIT), Harvard University, and the University of Waterloo. He has been a Full Professor of electrical engineering with Khalifa University (formerly, Etisalat University College), United Arab Emirates, which he joined in 1993 up to 2017, during which he received several times the Excellence in Teaching Award and Distinguished Service Award. He delivered more than 60 invited speaker seminars and technical talks in world-class universities and flagship conferences. He served as an Invited Speaker for the U.S. National Academies of Sciences, Engineering, and Medicine Frontiers Symposium. He has over 380 publications in the form of articles in peer-reviewed journals, papers in refereed conference proceedings, book chapters, and U.S. patents. His publication span several research areas, including 6G and terahertz communications, modern antennas and applied electromagnetics, signal and array processing, machine learning, the IoT and sensor localization, medical sensing, and nano-biomedicine. He is a fellow of the MIT Electromagnetics Academy and a Founding Member of the MIT Scholars of the Emirates. He is a standing member of the editorial boards of several international journals and serves regularly on the Steering, Organizing, and Technical Committees for IEEE flagship conferences in antennas, communications, and signal processing, including several editions of IEEE AP-S/URSI, EuCAP, IEEE GlobSIP, IEEE WCNC, and IEEE ICASSP. He is a Founding Member of five IEEE society chapters in United Arab Emirates, which are the IEEE Communication Society Chapter, the IEEE Signal Processing Society Chapter, the IEEE Antennas and Propagation Society Chapter, the IEEE Microwave Theory and Techniques Society Chapter, and the IEEE Engineering in Medicine and Biology Society Chapter. He was a recipient of several international awards, including the Distinguished Service Award from ACES Society, USA, and from the MIT Electromagnetics Academy, USA. He received the University of Waterloo Distinguished Doctorate Dissertation Award for the Ph.D. degree. He has served as the TPC Chair for IEEE MMS2016 and the TPC Chair for IEEE GlobalSIP 2018 Symposium on 5G Satellite Networks. He holds several leading roles in the international professional engineering community. He holds several leading roles in the international professional engineering community. He is a Board Member of the European School of Antennas and the Regional Director of the IEEE Signal Processing Society in IEEE Region 8 Middle East and served as the Founding Chair for the IEEE Antennas and Propagation Society Educational Initiatives Program. He is an Editor of the IEEE JOURNAL OF ELECTROMAGNETICS, RF, AND MICROWAVES IN MEDICINE AND BIOLOGY, and Editor of the IEEE OPEN JOURNAL OF ANTENNAS AND PROPAGATION. He is the Founder and the Chair of IEEE at New York University Abu Dhabi. He is an Officer for IEEE ComSoc Emerging Technical Initiative (ETI) on Machine Learning for Communications. He is the Founding Director of the IEEE UAE Distinguished Seminar Series Program for which he was selected to receive, along with Mohamed AlHajri of MIT, the 2020 IEEE UAE Award of the Year. He organized and chaired numerous technical special sessions and tutorials in IEEE flagship conferences.



VICTORIA RAMOS (Senior Member, IEEE) received the Ph.D. degree in biomedical engineering and telemedicine from the University of Alcalá, Madrid, Spain, in 2005. She was a Telecommunications Engineer with the Polytechnic University of Madrid. From 1985 to 1996, she worked as a Radio Communications Research and Development Engineer in the private industry. Since 1996, she has been a Research Scientist with the Instituto de Salud Carlos III,

where she is currently a Ph.D. Researcher, and a Civil Servant, belonging to the Ministry of Science, Innovation and University, in the research area of telemedicine and e-health, Madrid. Her objectives are to provide health care for mobile citizens and e-health focusing on new emergent health services based on telemedicine. It involves standards related to human exposure, medical devices immunity, and radio communication EMC. She is the author or has coauthored of several books as well as of several articles for scientific congresses. She takes part of several Spanish standardizations committees. Her research interests include wireless communications applications for home care and the next generations of sensors networks and body area networks and telemedicine applications.



FRANCISCO FALCONE (Senior Member, IEEE) received the degree in telecommunication engineering and the Ph.D. degree in communication engineering from the Universidad Pública de Navarra (UPNA), Spain, in 1999 and 2005, respectively. From February 1999 to April 2000, he was a Microwave Commissioning Engineer with Siemens-Italtel, deploying microwave access systems. From May 2000 to December 2008, he was a Radio Access Engineer with Telefónica

Móviles, performing radio network planning and optimization tasks in mobile network deployment. In January 2009, as a Co-Founding Member, he has been the Director of Tafco Metawireless, a spin-off company from the UPNA, until May 2009. In parallel, he was an Assistant Lecturer with the Electrical and Electronic Engineering Department, UPNA, from February 2003 to May 2009. In June 2009, he became an Associate Professor with the EE Department, and the Department Head, from January 2012 to July 2018. From January 2018 to May 2018, he was a Visiting Professor with the Kuwait College of Science and Technology, Kuwait. He is currently affiliated with the Institute for Smart Cities (ISC), UPNA, which hosts around 140 researchers. He is also acting as the Head of the ICT Section. He has over 500 contributions in indexed international journals, book chapters, and conference contributions. His research interests include computational electromagnetics applied to the analysis of complex electromagnetic scenarios, with a focus on the analysis, design, and implementation of heterogeneous wireless networks to enable context-aware environments. He received the CST 2003 and CST 2005 Best Paper Award, the Ph.D. Award from the Colegio Oficial de Ingenieros de Telecomunicación (COIT) in 2006, the Doctoral Award UPNA in 2010, the First Juan Gomez Peñalver Research Award from the Royal Academy of Engineering of Spain in 2010, the XII Talgo Innovation Award 2012, the IEEE 2014 Best Paper Award in 2014, the ECSA-3 Best Paper Award in 2016, and the ECSA-4 Best Paper Award in 2017.

• • •